

Using molecular dynamics to unravel phase composition behavior of nano-size pores in frozen soils: Does Young–Laplace equation apply in low temperature range?

Chao Zhang, Zhen Liu, and Peng Deng

Abstract: The phase composition curve of frozen soils is a fundamental relationship in understanding permafrost and seasonally frozen soils. However, due to the complex interplay between adsorption and capillarity, a clear physically based understanding of the phase composition curve in the low temperature range, i.e., <265 K, is still absent. Especially, it is unclear whether the Young–Laplace equation corresponding to capillarity still holds in nano-size pores where adsorption could dominate. In this paper, a framework based on molecular dynamics was developed to investigate the phase transition behavior of water confined in nano-size pores. A series of simulations was conducted to unravel the effects of the pore size and wettability on the freezing and melting of pore water. This is the first time that the phase composition behavior of frozen soils is analyzed using molecular dynamics. It is found that the Young–Laplace equation may not apply in the low temperature range.

Key words: frozen soils, molecular dynamics, pore size, phase composition curves, unfrozen adsorptive water, Young–Laplace equation, wettability.

Résumé : La courbe de composition de phase des sols gelés est une relation fondamentale dans la compréhension du pergélisol et des sols gelés selon la saison. Cependant, en raison de l'interaction complexe entre l'adsorption et la capillarité, une compréhension physique claire de la courbe de composition de phase dans la plage de basses températures, c'est-à-dire <265 K, est toujours absente. En particulier, il n'est pas clair si l'équation de Young–Laplace correspondant à la capillarité se maintient toujours dans les pores de taille nanométrique où l'adsorption pourrait dominer. Dans cette recherche, un cadre basé sur la dynamique moléculaire a été développé pour étudier le comportement de transition de phase de l'eau, confinée dans les pores de taille nanométrique. Une série de simulations a été menée pour démêler les effets de la taille et de la mouillabilité des pores sur la congélation et la fusion de l'eau interstitielle. C'est la première fois que le comportement de composition de phase des sols gelés est analysé, en utilisant la dynamique moléculaire. On trouve que l'équation de Young–Laplace peut ne pas s'appliquer dans la plage des basses températures. [Traduit par la Rédaction]

Mots-clés : sols gelés, dynamique moléculaire, taille des pores, courbes de composition de phase, eau adsorbée non congelée, équation de Young–Laplace, mouillabilité.

Introduction

In the northern hemisphere, approximately 26% of the land surface is occupied by permafrost regions (Zhang et al. 2003). Therefore, the behavior of geomaterials in cold environments is a continuous issue challenging researchers and engineers. For example, the presence of ice in soils will significantly reduce their hydraulic conductivities and increase their shear strength (Painter and Karra 2014), which is of critical importance to assess the performance of infrastructures and geo-hazards in cold regions.

The freezing and melting temperatures of pore water are different from those of pure bulk water due to the temperature depression effect caused by the confinements of narrow pores (Alba-Simionesco et al. 2006). The Clapeyron equation is widely adopted to depict this depression effect in terms of water and ice pressure differences (e.g., Williams and Smith 1989; Sheng et al. 2013; Painter and Karra 2014; Zhang et al. 2016c). The temperature depression could be calculated using a generalized form of the

Clapeyron equation (e.g., Konrad and Morgenstern 1980, 1981; Watanabe and Flury 2008; Liu and Yu 2013):

$$(1) \quad T = T_0 \exp\left(\frac{\psi}{-\rho_w L_a}\right)$$

where T_0 is the freezing point of pure bulk water ($= 273.15$ K); ψ is matric suction; ρ_w is the density of water ($= 1.0 \times 10^3$ kg/m³); and L_a is the latent heat of water fusion ($= 3.34 \times 10^5$ J/kg).

By combining eq. (1) with the soil water characteristic curve (SWCC), a mathematical model that relates the unfrozen water content to the temperature can be obtained (Painter and Karra 2014), which is referred to as the phase composition curve (PCC) (Liu and Yu 2013). The applicability of this approach has been validated by a group of researchers in saturated frozen soils (e.g., Koopmans and Miller 1966; Spaans and Baker 1996). Despite these experimental validations, there are still some problems in need of clarifications. Due to the similarity in physical mechanisms, the SWCC was found to be analogous to the soil freezing characteris-

Received 16 March 2016. Accepted 3 August 2017.

C. Zhang and P. Deng. Department of Civil and Environmental Engineering, Colorado School of Mines, Golden, CO 80401, USA.

Z. Liu. Department of Civil and Environmental Engineering, Michigan Technological University, Houghton, MI 49931, USA.

Corresponding author: Zhen Liu (email: zhenl@mtu.edu).

Copyright remains with the author(s) or their institution(s). Permission for reuse (free in most cases) can be obtained from [RightsLink](https://www.rightslink.com).

tic curve (SFCC) (e.g., Koopmans and Miller 1966; Spaans and Baker 1996), which is the reason why a PCC was usually obtained by combining eq. (1) with the SWCC of the same soil. In the high suction range of SWCCs, adsorption rather than capillarity dominates matric suction (Lu and Likos 2004). As a result, conventional SWCC models are not capable of accurately capturing the soil-water characteristics in the high suction range (Webb 2000; Likos and Yao 2014). As for frozen soils, the high suction range of SWCCs corresponds to the low temperature range of their SFCCs. Therefore, it remains obscure whether the aforementioned method is applicable to describing the phase composition behavior in the low temperature range.

In addition to SWCCs, the bundle of cylindrical capillary (BCC) model has been frequently adopted as a conceptual model to interpret the behavior of both partially saturated and partially frozen soils (e.g., Mualem 1976; Watanabe and Flury 2008; Liu and Yu 2013). By employing the BCC model, the Clapeyron equation and the capillary condensation relationship (Young–Laplace equation), a closed-form mathematical model could be derived for the PCC. Liu and Yu (2013) selected the Young–Laplace equation (Young 1805; Laplace 1806) to represent the matric suction in capillary tubes as

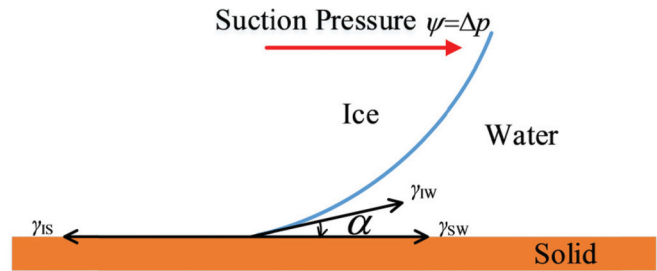
$$(2) \quad \psi = \Delta p = \gamma \nabla \cdot \mathbf{n}$$

where Δp is the pressure difference across the water–ice interface; γ is the surface tension on the water–ice interface; \mathbf{n} is the unit outward normal vector of the interface. It is well acknowledged that the adsorptive effect, which is not considered in the Young–Laplace equation, could dominate matric suction in minuscule pores (e.g., Or and Tuller 1999; Bachmann and van der Ploeg 2002). Therefore, this approach is still incomplete for describing the PCC in the low temperature range.

Molecular dynamics (MD) simulation has been recognized as an efficient tool to investigate complex physical and chemical processes. It has been successfully implemented to study the phase transition of water (e.g., Koga et al. 2001; Gonzalez Solveyra et al. 2011; Moore and Molinero 2011; Moore et al. 2012). Koga et al. (2001) utilized MD simulations to study the phase behavior of water encapsulated in carbon nanotubes. Moore et al. (2012) investigated the temperature depression effects of water confined in amorphous nanopores. Their MD simulations have shown excellent performance in predicting the ice nucleation and melting temperature in the nano-size pores (Gonzalez Solveyra et al. 2011; Moore et al. 2012). In the geotechnical community, MD simulations have already been applied to understand some complex soil problems, such as the seepage and diffusion behavior of clay minerals (e.g., Ichikawa et al. 2002; Bourg and Sposito 2010), the mechanical behavior of clay minerals (e.g., Katti et al. 2007, 2015), multi-scale modeling of geomaterials (Song et al. 2007), and the meniscus of the capillary water between clay particles (Amarasinghe and Anandarajah 2011; Anandarajah and Amarasinghe 2011; Zhang et al. 2017b). However, these existing studies have not addressed the influence of pore size on the temperature depression effect and the interplay of adsorption and capillarity, which is critical to understanding the behavior of frozen soils.

To obtain a physically based PCC model, it is indispensable to express matric suction, ψ , as a function of common soil properties, such as pore-size distribution, wettability, and pore shape. With a value greater than 10.0 MPa, matric suction lies in the “tightly adsorptive regime” of SWCCs where adsorption dominates matric suction (McQueen and Miller 1974; Lu and Likos 2004). According to eq. (1), such a high suction could depress the freezing and melting points to a value <265 K. For convenience, we will call temperatures <265 K as the “low temperature range” in this paper. Neither conventional SWCC models nor the Young–Laplace equation could well represent the frozen soil behavior in

Fig. 1. Conceptual model of ice–water–solid interfacial tension (modified from Liu et al. 2003) and matric suction. [Color online.]



the low temperature range due to the complex interplay of adsorption and capillarity. Instead, the phase behavior of water confined in nano-size pores (nanopore) in soils, possibly including both capillarity and adsorption, governs the PCC in the low temperature range. According to eq. (2), the diameter of such pores is approximately estimated to be <10 nm. Therefore, an investigation into the freezing and melting of water confined in nanopores is a necessary step forward towards a thorough understanding of the PCC in the low temperature range. In this study, the phase behavior of water confined in nanopores was investigated using MD simulations. The nanopores were represented by cylindrical tubes with nano-size dimensions corresponding to the low temperature range of the PCC. A series of parametric studies was conducted to investigate the influence of the pore size and wettability.

Physical origin of temperature depression effect

The surface energy of ice is much different from that of liquid water. Therefore, the ice–water–solid interface can be highly curved and form an acute contact angle. As shown in Fig. 1, a contact angle of α is formed at the ice–water–solid interface due to the interaction among the ice–solid surface tension γ_{is} , the ice–water surface tension γ_{iw} , and the solid–water surface tension γ_{sw} . Because the surface energy of ice is higher than that of water, the ice–water interface is usually convex and α is around 0° . According to the Young–Laplace equation, a pressure difference or matric suction will develop across the ice–water interface, leading to the fact that the ice phase exhibits a higher pressure than water.

The phase behavior of pore water can be explained using a phase diagram that depicts the phase behavior as a function of the pressure, P , and temperature, T . A typical phase diagram for water is illustrated in Fig. 2 (Çengel et al. 2004). The red lines in the diagram mark the transition boundaries between different phases. The axis translation technique (Lu and Likos 2004) then can be used to extend this diagram from pure bulk water to pore water. That is, the pressure in liquid water is assumed to be fixed at a reference pressure such as one atmosphere while the ice pressure is increased to maintain the pressure difference. As shown in Fig. 2, the pressure of the ice confined in pores is larger than the atmospheric pressure due to the matric suction. Along the boundary between the ice and liquid water, the phase transition temperature, i.e., melting temperature, decreases with the increase in pressure. As a result, the melting point of the ice confined in nanopores is depressed to a value <273.15 K. This physical phenomenon can be quantified via the Clapeyron equation (eq. (1)).

As for the conceptual model in Fig. 1, it is feasible to adopt the Young–Laplace equation to represent matric suction, ψ . Then, a mathematical model for the temperature depression effect could be conveniently obtained with the aid of the Clapeyron equation. However, it is questionable whether the conceptual model in Fig. 1 still holds in nano-size pores where the ice–water–solid interfacial interactions are much more complex. Figure 3 schemat-

Fig. 2. Conceptual illustration of the temperature depression effect in the phase diagram of water. D , pore diameter. (1 atm = 101.325 kPa) [Color online.]

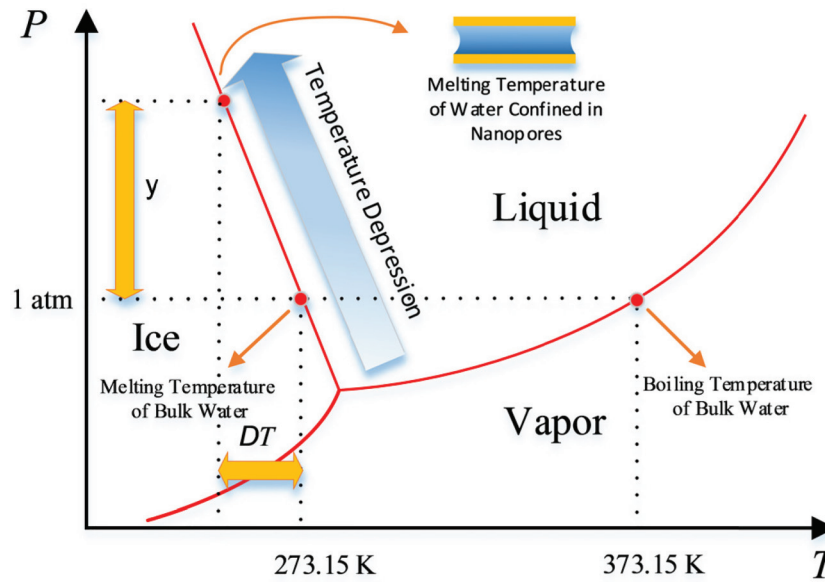
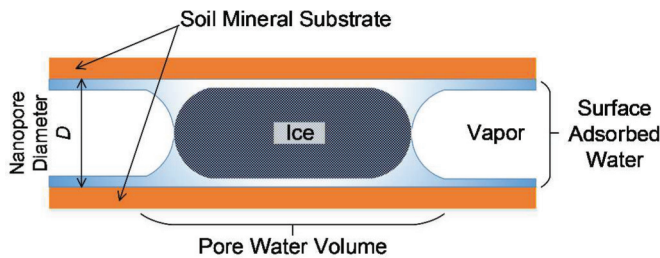


Fig. 3. Schematic diagram of phase arrangement in confined water (modified from Findenegg et al. 2008). [Color online.]



ically depicts the phase arrangement in a partially filled nanopore (Findenegg et al. 2008). It could be observed that vapor, liquid water, and ice may coexist in the nanopore within a certain temperature range. Moreover, adsorptive water does not freeze, but instead, forms a thin film between the solid and ice (Mitchell and Soga 2005). The thickness of adsorptive water was found to be 0.5–1.0 nm (Anderson and Hoekstra 1965). Therefore, adsorption may have a significant effect and thus cannot be ignored in nanosize pores.

Models and methods

Force field and molecular model

Various water models have been proposed for the molecular modeling of water, such as the simple point charge (SPC) model (Berendsen et al. 1981), the extended simple point charge (SPC/E) model (Berendsen et al. 1987), the three point transferable intermolecular potential (TIP3P) model, and the four point transferable intermolecular potential (TIP4P) model (Jorgensen et al. 1983). Most of these atomistic water models could not well reproduce the crystal structures and phase transition behavior of water (Moore et al. 2010). Also, the computational costs of these atomistic models are remarkably high due to the need to calculate the long-range Coulombic force (Molinero and Moore 2009; Moore et al. 2010). Molinero and Moore (2009) developed the monoatomic water model (mW model), i.e., a coarse-grained water model, to speed up the computational time under the premise of well reproducing the thermodynamic properties, structural anomalies and phase transition behavior of water. In the mW

model, the water–water interaction is modeled by only short-range interactions based on the similarities between water and silicon. As a result, the calculation of the long-range Coulombic force is avoided, and the computational cost is significantly reduced. A detailed justification of the mW model can be found in Molinero and Moore (2009). Recently, the mW model has been widely adopted to investigate various behaviors of confined water, e.g., sorption isotherms (De La Llave et al. 2012), phase transitions (Moore et al. 2012), and effective stress evolution (Zhang et al. 2016b).

In this study, the mW model was selected considering its accuracy and relatively low computational costs. The mW model can be represented by the Stillinger–Weber potential (Stillinger and Weber 1985) as a combination of the pairwise potential, ϕ_2 , and three body potential, ϕ_3

$$(3) \quad E = \sum_i \sum_{j>i} \phi_2(r_{ij}) + \sum_i \sum_{j \neq i} \sum_{k>j} \phi_3(r_{ij}, r_{ik}, \theta_{ijk})$$

$$(4) \quad \phi_2(r_{ij}) = A\varepsilon \left[B \left(\frac{\sigma}{r_{ij}} \right)^{p_{ij}} - \left(\frac{\sigma}{r_{ij}} \right)^{q_{ij}} \right] \exp\left(\frac{\sigma}{r_{ij} - a\sigma} \right)$$

$$(5) \quad \phi_3(r_{ij}, r_{ik}, \theta_{ijk}) = \lambda\varepsilon(\cos\theta_{ijk} - \cos\theta_0)^2 \exp\left(\frac{\gamma\sigma}{r_{ij} - a\sigma} + \frac{\gamma\sigma}{r_{ik} - a\sigma} \right)$$

where ϕ_2 defines a pairwise interaction between water molecules; r_{ij} is the distance between atom i and atom j ; ϕ_3 is a repulsive three-body potential to penalize configurations with nontetrahedral angles and thus controls the crystallization of water; θ_{ijk} is the angle between the vectors r_{ij} and r_{ik} ; $A = 7.049\,556\,277$; ε is the energy scale of the pairwise interaction ($= 6.189$ kcal/mol); $B = 0.602\,224\,558\,4$; σ is the length scale of the pairwise interaction ($= 2.3925$ Å) and therefore controls the equilibrium distance between water molecules; $p_{ij} = 4$; $q_{ij} = 0$; $a = 1.8$; λ denotes the strength of the repulsive three-body potential ($= 23.15$) and is referred to as the tetrahedrality parameter; θ_0 is the “ideal” tetrahedral angle ($= 109.47^\circ$); $\gamma = 1.2$.

In a water–nanopore system, three types of interatomic interactions need to be considered: the water–water interaction, the nanopore–nanopore interaction, and the water–nanopore interaction. All these interatomic interactions were modeled in terms

Fig. 4. Variation of pore wettability with water–nanopore interaction characteristic energy ϵ_{wn} . Red dots and blue dots represent solid atoms and water molecules, respectively. [Color online.]

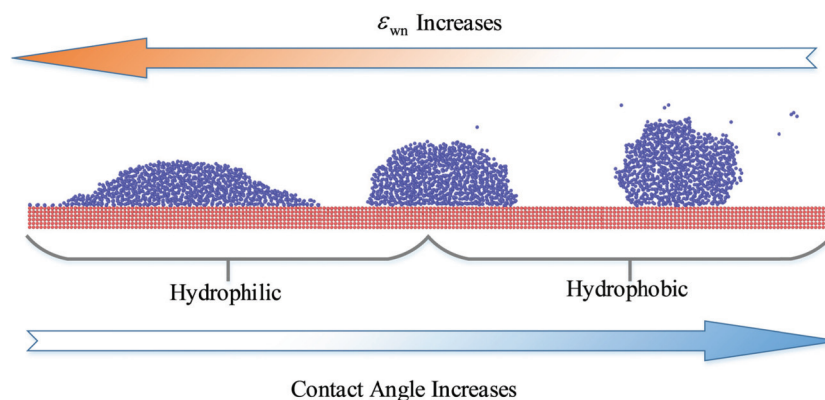
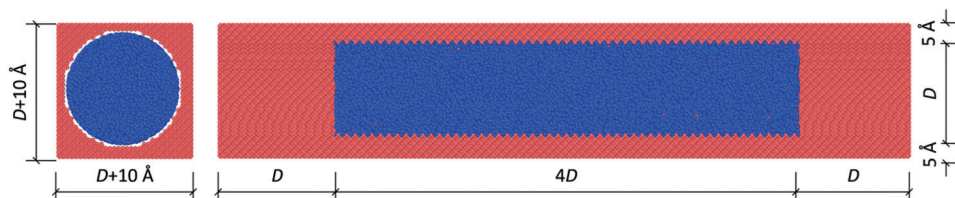


Fig. 5. Initial configuration of simulated water–nanopore system. Red dots and blue dots represent solid atoms and water molecules, respectively. [Color online.]



of the Stillinger–Weber potential (eqs. (3)–(5)). The difference between the potentials for different types of interaction lies in the values of the tetrahedrality parameter λ , the length scale σ , and the energy scale ϵ . For clarity, the tetrahedrality parameter, length scale, and energy scale for the water–nanopore interaction were denoted as λ_{wn} , σ_{wn} , and ϵ_{wn} , respectively. The default values in the original mW model were used for the water–water interaction and the nanopore–nanopore interaction while adjusted values were adopted for the water–nanopore interaction (Moore et al. 2012). The parameter σ_{wn} was set to 3.2 Å to eliminate the diffusion of water atoms into the nanopores. The parameter λ_{wn} was set as 0.0 to reduce the tetrahedrality of the potential. The wettability of nanopores was controlled by the values of the characteristic energy ϵ_{wn} . The adopted values of ϵ_{wn} are 0.3, 0.4, 0.6, and 0.7 kcal/mol. The variation of the wettability with the water–nanopore interaction characteristic energy ϵ_{wn} is schematically shown in Fig. 4.

Initial configuration

As illustrated in Fig. 5, the initial configuration of the simulated water–nanopore system is a cylindrical nanotube filled with a body of water. The water body was placed at the center of the nanopore. The dimensions of the simulation cell were set to $6D \times (D + 10 \text{ \AA}) \times (D + 10 \text{ \AA})$, where D is the diameter of the pore. The exact dimensions were adjusted to be integer multiples of the lattice constants of the solid.

The primary aim of this study is to elucidate the influence of adsorption on the temperature depression and investigate the validity of the Young–Laplace equation in the low temperature range. The face-centered cubic (FCC) crystal structure is ubiquitous in engineering practice and frequently selected to test the validity of classical theories or equations (e.g., Luan and Robbins 2005; Cheng and Robbins 2014). Therefore, the nanopore was modeled as an FCC crystal structure herein to preliminarily answer whether Young–Laplace equation applies in the low temperature range. At first, the FCC crystal unit cells were stacked along the x -, y -, and z -directions to reach a size around $6D \times (D + 10 \text{ \AA}) \times (D + 10 \text{ \AA})$. Then a cylindrical nanopore with a diameter of D was

carved at the center of the supercell. It should be noted that the length of the nanopore can be regarded as infinite with the aid of periodic boundary conditions. A harmonic bond was added between the nanopore (solid) atoms to retain the FCC structures during the simulation process (Luan and Robbins 2005). The equilibrium length of the bond was identical to the parameter σ . The spring constant for the harmonic bond was calibrated as 60 kcal/mol. To investigate the nanopore size effects, six nanopore diameters were used: 1, 2, 3, 4, 5, and 6 nm. According to eq. (2), the upper bound of the “low temperature range”, i.e., 265 K, approximately corresponds to the matrix suction provided by the nanopore with a diameter of 10 nm. Therefore, it is better to extend the simulated nanopore diameter to 10 nm. However, even with the mW model, the computational cost for this kind of MD simulation is still tremendously expensive. For example, it took approximately 33 days to finish one $D = 6$ nm simulation case with 64 CPU cores (Intel Sandy Bridge E5-2670 2.60 GHz). Therefore, the maximum nanopore diameter adopted for the MD simulations was 6 nm in this study.

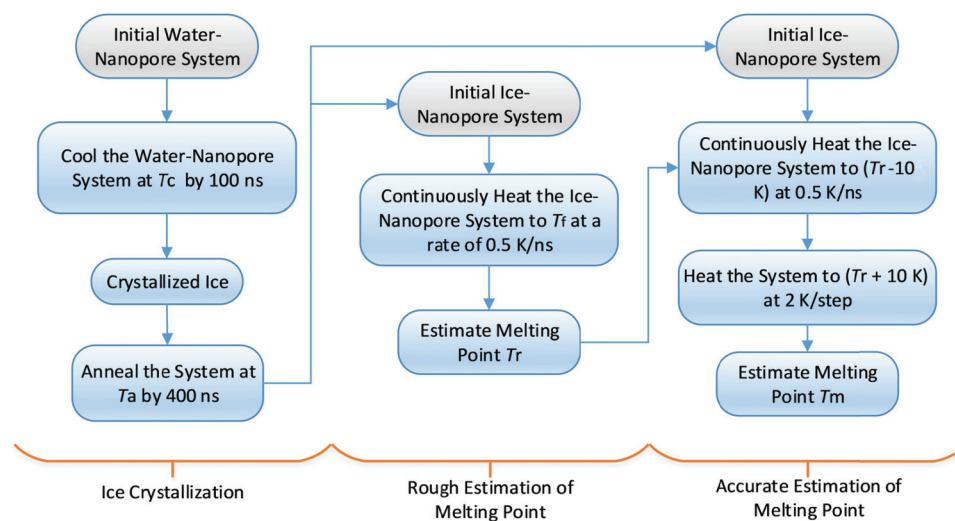
The initial configuration of the water body was generated by the packing optimization for molecular dynamics simulations (PACKMOL) (Martínez et al. 2009), which is an open-source package developed for generating good initial configurations without disrupting simulations. The initial configuration of the water body was modeled as a cylinder. The diameter of the water cylinder was set as $D-3.1 \text{ \AA}$, which is a little smaller than that of the nanopore, to avoid a bad initial configuration. The length of the water cylinder was set as $4D$, which is smaller than the length of the nanopore ($6D$) to reserve extra space for the water expansion upon freezing. The number of water molecules to fill in the cylinder was determined by ensuring that the pore water has the same density as bulk liquid water.

Simulation setups

Quantification of nanopore wettability

A quantitative analysis is firstly needed to relate the wettability of nanopores to the characteristic interaction energy ϵ_{wn} . The

Fig. 6. Flowchart of simulation procedure. [Color online.]



contact angle was selected as the indicator to quantify the wettability. The contact angles of nanopores were determined using an MD simulation method reported in Zhang et al. (2016a). In this method, the initial simulation system was set up as a body of water placed above an infinite nanopore slab and referred to as the sessile droplet system. The system was equilibrated under a constant number of particles, volume, and temperature (NVT) ensemble at a constant temperature of 300 K. The simulations were run for a process of 3 ns with an integration time step of 1.0 fs. The molecular trajectories in the last 2 ns were recorded to determine the time average density profiles that were later used for the determination of contact angles. More detailed simulation settings and procedure for determining contact angles could be found in Zhang et al. (2016a).

Simulations of freezing and melting process

The freezing and melting simulations of the water–nanopore system were conducted under the constant number of particles, pressure, and temperature (NpT) ensemble at $p = 1.0$ atm and varying temperatures. As shown in Fig. 6, three steps of MD simulations, i.e., ice crystallization, rough estimation of melting point, and accurate estimation of melting point, were adopted to investigate the freezing and melting behavior of the water–nanopore systems. First, the initial water–nanopore system was equilibrated at a constant temperature of T_c for 100 ns. During this step, the water confined in the nanopores crystallized. However, the crystallized ice consisted of different types of ice structures. To obtain a single crystallite ice, the system was further annealed under the NpT ensemble at a slightly higher temperature of T_a for 400 ns (Moore et al. 2012). Then the ice crystallization step was finished and the initial ice–nanopore system was obtained. Second, the obtained initial ice–nanopore systems were continuously heated under NpT ensemble from T_a to the final temperature in the heating step, T_f , at a rate of 0.5 K/ns. For every snapshot, the amount of ice was identified to quantify the phase transition of water. The ice structure identification was carried out using the common neighbor analysis (Honeycutt and Andersen 1987), which is an algorithm aimed to characterize local crystal structures. A detailed description of the common neighbor analysis can be found in Honeycutt and Andersen (1987) and Faken and Jónsson (1994). This algorithm has been implemented in the open visualization tool (OVITO) (Stukowski 2010). The melting point could be roughly estimated as the temperature T_r at which all the ice melts. Third, the obtained initial ice–nanopore system from the first step was continuously heated from the temperature T_a to the temperature $T_r - 10$ K at a rate of 0.5 K/ns. Then the system was heated to $T_r +$

Table 1. Values of T_c , T_a , and T_f for nanopores with different pore diameters.

Temperature (K)	Pore diameter, D					
	1 nm	2 nm	3 nm	4 nm	5 nm	6 nm
T_c	100	150	170	180	185	190
T_a	120	170	190	200	205	210
T_f	170	220	240	250	255	260

Note: T_c , constant temperature; T_a , annealed temperature; T_f , final temperature in heating step.

10 K by 2 K at a time. At each temperature increment, the system was equilibrated for 50 ns. The melting point could be accurately determined as the temperature T_m at which the amount of ice turns into zero. It should be noted that the values of T_c , T_a , and T_f are different for nanopores with different pore diameters, which are summarized in Table 1.

The boundaries in all the directions of the simulation box were set as periodic to reduce the surface effect (Liu et al. 2004). All the MD simulations were conducted with the large-scale atomic/molecular massively parallel simulator (LAMMPS) distributed by the Sandia National Laboratories (Plimpton 1995; Plimpton et al. 2007) and visualized with the OVITO (Stukowski 2010). The Newton's equations of motion were integrated with a time step of 10.0 fs.

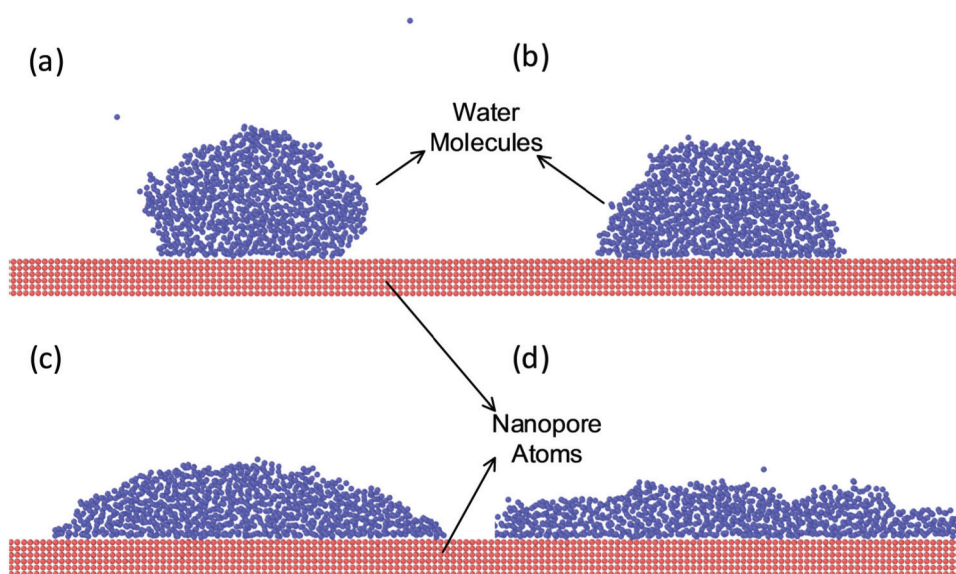
Results and discussions

Wettability of nanopores with different characteristic interaction energies

The water droplet was placed on the nanopore slabs with a characteristic interaction energy of 0.3, 0.4, 0.6, and 0.7 kcal/mol. It is expected that the simulated systems reached statistical equilibrium after 1 ns when the total potential energy kept fluctuating around a certain value. Therefore, the molecular trajectories in the last 2 ns can be used to determine time average density profiles. Figure 7 shows the snapshots of the sessile droplet systems in equilibrium. It can be observed that the contact area between the droplet and nanopore slab increases with an increasing ϵ_{wn} , supporting the assumption that the wettability can be changed by adjusting ϵ_{wn} . The nanopore with $\epsilon_{wn} = 0.3$ kcal/mol was typically hydrophobic while the nanopores with $\epsilon_{wn} = 0.6$ or 0.7 kcal/mol were hydrophilic.

The contact angle between the water–vapor interface and the solid surface was selected as the indicator of wettability of the nanopore and was determined using the method proposed in

Fig. 7. Snapshots of sessile droplet systems at equilibrium for $\epsilon_{wn} =$ (a) 0.3 kcal/mol, (b) 0.4 kcal/mol, (c) 0.6 kcal/mol, and (d) 0.7 kcal/mol. Red dots and blue dots represent solid atoms and water molecules, respectively. [Color online.]



Zhang et al. (2016a). It is worthwhile to mention that this contact angle is different from the contact angle mentioned in section titled “Physical origin of temperature depression effect”, the angle that is formed by the ice–water interface and solid surface. Figure 8 illustrates the determination of the contact angles of the sessile droplet systems with different ϵ_{wn} values. The contact angles were measured as 112° with $\epsilon_{wn} = 0.3$ kcal/mol, 82° with $\epsilon_{wn} = 0.4$ kcal/mol, 49° with $\epsilon_{wn} = 0.6$ kcal/mol, and 26° with $\epsilon_{wn} = 0.7$ kcal/mol. Compared with the simulation results from Zhang et al. (2016a), the contact angles of the nanopores with $\epsilon_{wn} = 0.6$ and 0.7 kcal/mol are analogous to those of α -quartz and orthoclase while the contact angle of the nanopore with $\epsilon_{wn} = 0.3$ kcal/mol is analogous to that of muscovite. Therefore, it is reasonable to use these nanopores to represent the wettability of soil minerals.

Effects of wettability of nanopores

The freezing and melting simulations were performed on the water–nanopore systems with a diameter of 4 nm and varying ϵ_{wn} values, i.e., 0.3, 0.4, 0.6, and 0.7 kcal/mol, to examine the influence of the nanopore wettability on the phase behavior of the pore water. Figure 9 shows the representative snapshots of the melting processes of crystallized ice in the nanopores with $\epsilon_{wn} = 0.3$ and 0.7 kcal/mol. As can be seen, more water molecules were adsorbed to the nanopore surface with $\epsilon_{wn} = 0.7$ kcal/mol than that with $\epsilon_{wn} = 0.3$ kcal/mol as a result of its higher characteristic interaction energy. It is interesting to point out that the water molecules adsorbed to the nanopore surface outside the bulk water could not crystallize even under extremely low temperatures. To confirm this, we cooled the water–nanopore system to 50 K and equilibrated for 400 ns. No crystal structures of ice were observed in the adsorptive water molecules outside the bulk water. This observation confirms the existence of the pre-melted adsorptive water layer in the nanopore surface (e.g., Iwata et al. 1995; Mitchell and Soga 2005). As temperature increased, the pre-melted adsorptive water layer between the ice and nanopore surface became thicker and thicker. Meanwhile, the ice in contact with the vacuum transformed into liquid water at first and then gradually formed a thin liquid water film, which is consistent with the conceptual model depicted in Fig. 3. Eventually, all the ice turned into the liquid phase at a temperature that was identified as the melting point. The melting points in moderately hydrophobic and hydrophilic nanopores, i.e., $\epsilon_{wn} = 0.4$ and 0.5 kcal/mol, were both 222 K. However, the melting points in strongly hydrophilic and hydrophobic

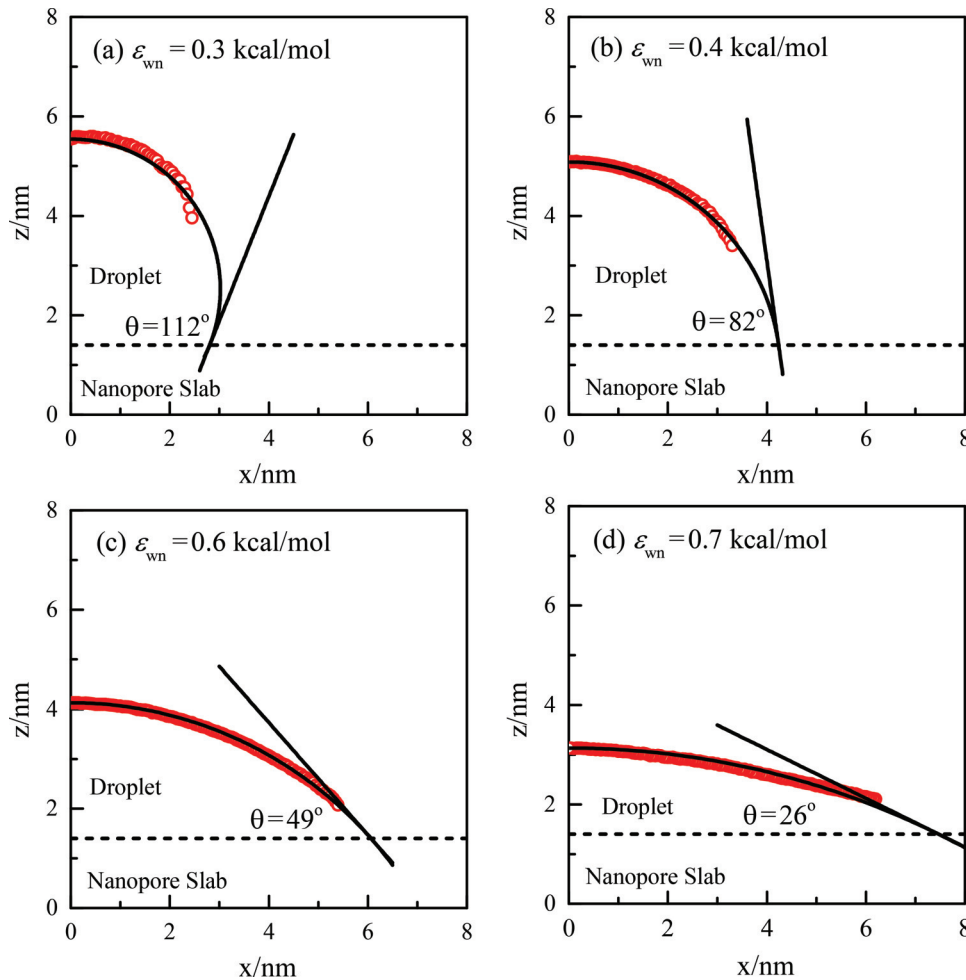
cases slightly decreased and increased, respectively: 218 K for $\epsilon_{wn} = 0.3$ kcal/mol and 226 K for $\epsilon_{wn} = 0.7$ kcal/mol. These results are qualitatively consistent with the observation of Moore et al. (2012) on the amorphous nanopores.

Figure 10 illustrates the unfrozen water fraction – temperature curves with different nanopore wettabilities. The unfrozen water fraction was determined by a time average over the last 10 ps of every temperature step. In general, as the contact angle increased, the initial unfrozen water fraction decreased due to the fact that fewer water molecules were adsorbed to the nanopore surface. The unfrozen water fraction gradually increased with an increase of temperature as a result of the thickening of the premelted water layer on the ice–vacuum and ice–nanopore interfaces. Around one certain temperature threshold, the unfrozen water fraction rapidly increases to 1.0. This temperature threshold was identified as the melting point. It could be observed that the melting point increased by 4 K with increasing wettability, which is consistent with the observation in Fig. 9.

Effects of nanopore size

Nanopores with six different diameters, i.e., 1, 2, 3, 4, 5, and 6 nm, were adopted to investigate the effects of nanopore size. The characteristic interaction energy ϵ_{wn} was fixed at 0.6 kcal/mol. Figure 11 illustrates a sectional view of the crystallized ice in the nanopores with different diameters at T_c . In the last four cases, it can be observed that most of the confined water transformed into crystal ice except some water molecules adsorbed on the surface. However, no stable crystal structures were identified in the nanopores with a diameter of 1 and 2 nm. This interesting phenomenon could be attributed to the dominant effect of adsorption. Within a smaller nanopore, a larger portion of water molecules is dominated by the water–nanopore interaction, i.e., the adsorptive effect. The adsorptive effect will arrange the water molecules into some regular molecular layers as observed in Zhang et al. (2016a). In Figs. 11a–11b, it can be observed that the confined water molecules are arranged in some orders. The free energy of these ordered water molecules is much lower than that of pure bulk water. Previous studies have shown that the free energy of adsorptive water can be 8.62 kcal/mol lower than pure bulk water (Zhang et al. 2017a). When these ordered water molecules exhibit a lower free energy than ice, they are more energetically favored than ice and thus cannot form ice crystals (Anderson 1967). To confirm this, the water–nanopore systems with $D = 1$ and 2 nm were equil-

Fig. 8. Determination of contact angles of sessile droplet systems, θ , for $\varepsilon_{wn} =$ (a) 0.3 kcal/mol, (b) 0.4 kcal/mol, (c) 0.6 kcal/mol, and (d) 0.7 kcal/mol. Dashed line represents surface of nanopore slab. [Color online.]



ibrated at an extremely low temperature of 50 K, but there was still no ice crystal structures. Therefore, it may be concluded that the water confined in the nanopores with a diameter smaller than a certain value (probably a value between 2 and 3 nm) cannot be frozen. With the aid of the BCC model, it may be inferred that soils cannot be further frozen below a certain temperature at which most capillary water has turned into ice.

To quantify the effect of the nanopore diameter, unfrozen water fraction – temperature curves with different nanopore diameters are compared in Fig. 12. It could be observed that the unfrozen water fraction at T_c decreases with the increase of nanopore diameter, which could be attributed to the weakening of the adsorptive effect. The melting point increased with the increase of nanopore diameter, which is consistent with existing theories (Liu and Yu 2013). As for the nanopore with $D = 3$ nm, the melting point could be depressed by 57 K from that of pure bulk water.

Comparisons with Young–Laplace–Clapeyron method

As mentioned in section titled “Introduction”, the temperature depression effect can be expressed as a function of matric suction in terms of the Clapeyron equation (eq. (1)). If neglecting the adsorptive effect, matric suction can be expressed as a function of the nanopore diameter with the aid of the Young–Laplace equation (eq. (2)). For a cylindrical nanopore, eq. (2) can be rewritten as

$$(6) \quad \psi = \Delta p = \frac{4\gamma \cos\alpha}{D}$$

where α is the ice–water–solid interface contact angle (shown in Fig. 1) and can be assumed to be 0° for simplicity. Substituting eq. (6) into eq. (1), the melting point could be expressed as a function of the nanopore diameter as

$$(7) \quad T = T_0 \exp\left(\frac{4\gamma \cos\alpha}{-\rho_w L_a D}\right)$$

Herein, this way to predict the temperature depression effect is referred to as the Young–Laplace–Clapeyron method. Figure 13 illustrates the comparisons of the melting points predicted using the Young–Laplace–Clapeyron method and those from the MD simulations. It could be observed that the prediction with the Young–Laplace–Clapeyron method generally tends to underestimate the melting temperature depression. The prediction error could be as large as 22–25 K for nanopores when compared with MD simulation results. This error was likely caused by the adsorptive effect. In addition, according to the MD simulations, there exists a region, i.e., $D \leq 2$ nm, where pore water cannot freeze. This region can be distinguished by a temperature point that is referred to as the “unfreezable temperature threshold”. Below this threshold, all freezable pore water in soils has been transformed into ice, and the remaining liquid pore water will only undergo supercooling. By fitting the MD simulation results with an exponential curve, the “unfreezable temperature threshold” could be roughly estimated as 200 K. However, more accurate determina-

Fig. 9. Representative snapshots of melting processes of crystallized ice in nanopores. Upper series of snapshots represents case with $\epsilon_{wn} = 0.3$ kcal/mol while lower series of snapshots represents case with $\epsilon_{wn} = 0.7$ kcal/mol. Grey dots and blue dots represent water molecules and ice molecules, respectively. [Color online.]

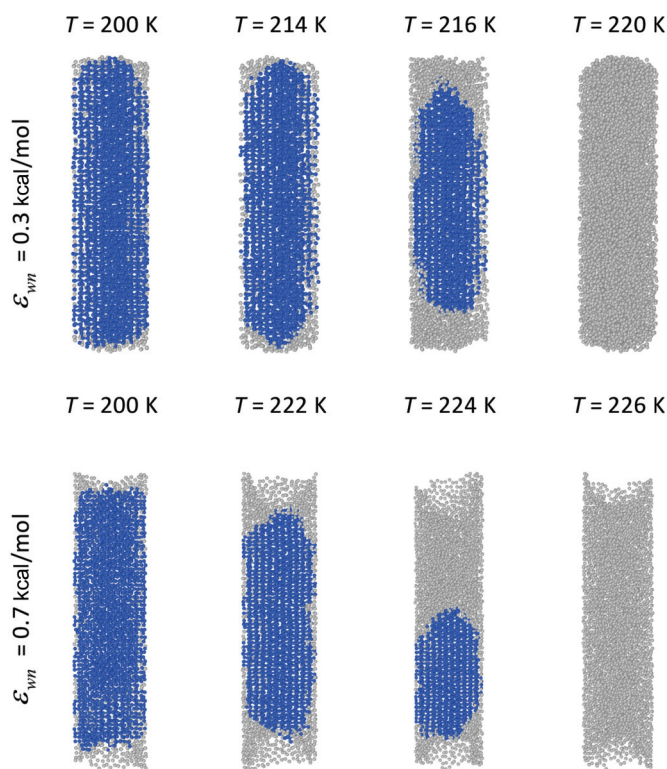
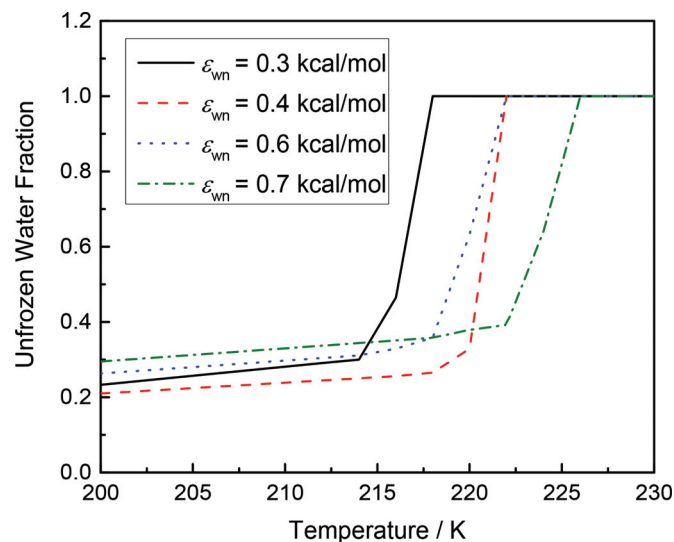


Fig. 10. Unfrozen water fraction – temperature curves with different nanopore wettability. [Color online.]



tion of its value needs further well-designed MD simulations that are beyond the scope of this study. Evidently, this region is dominated by adsorption thus cannot be predicted using the Young–Laplace–Clapeyron method. Therefore, it is concluded that adsorption is not negligible in nano-size pores that govern the low-temperature range in the PCC of frozen soils. This conclusion may also apply to the SWCC of unsaturated soils in the high suction range.

Fig. 11. Sectional view of crystallized ice in nanopores with different diameters under T_c . Red dots, grey dots, and blue dots represent solid atoms, water molecules, and ice molecules, respectively. [Color online.]

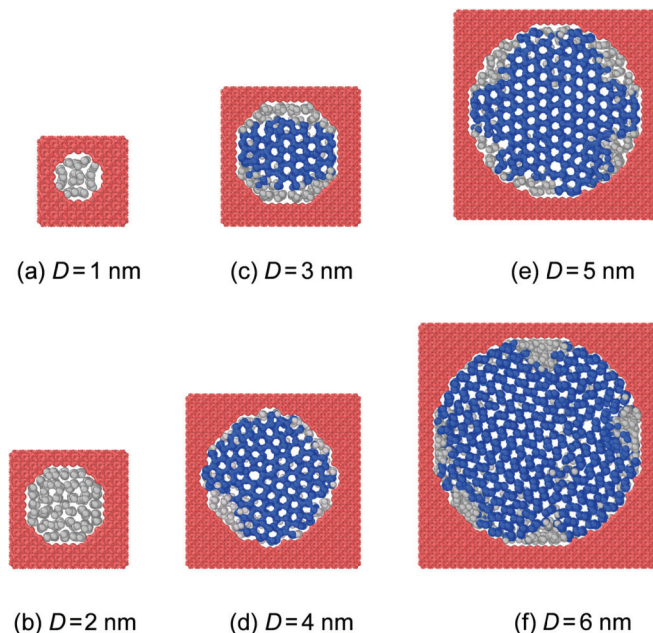
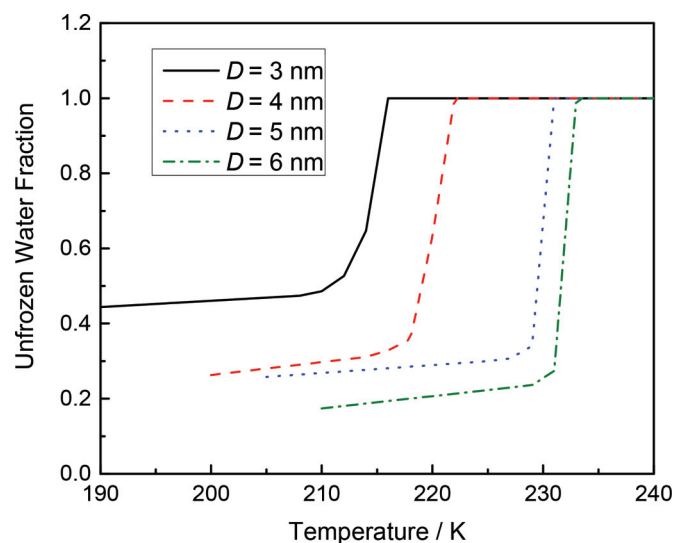
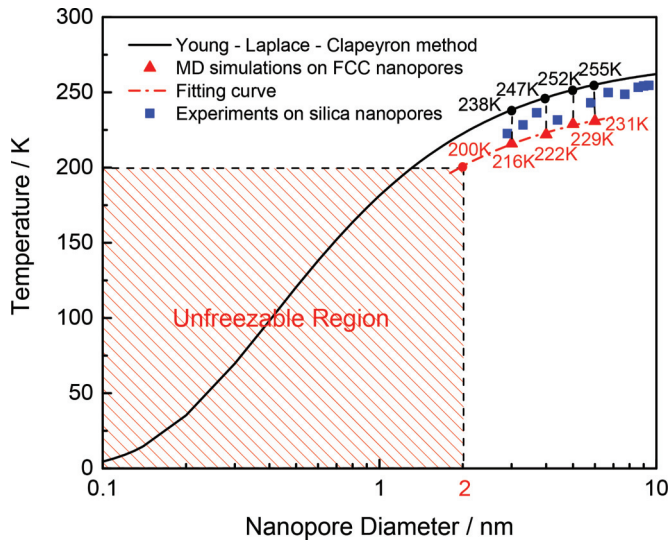


Fig. 12. Unfrozen water fraction – temperature curves with different nanopore diameters. [Color online.]



To further justify the conclusion, the experiment results in silica nanopores reported by [Schreiber et al. \(2001\)](#) are illustrated in [Fig. 13](#). For all experimental cases, the Young–Laplace–Clapeyron method underestimates the temperature depression effects, which is consistent with the MD simulations. In general, the deviations between the experimental results and the Young–Laplace–Clapeyron method tend to decrease with the nanopore diameter, confirming the hypothesis that adsorption plays a more significant role in smaller pores. The melting points from experimental results are slightly higher than MD simulations. This may be attributable to the FCC crystal solid in MD simulations being more rigid than the amorphous silica. During the freezing process, the volume expansion of ice crystals needs to be compatible with the crystal surface topography. Therefore, solid properties may influence the phase

Fig. 13. Melting points predicted using Young–Laplace–Clapeyron method, molecular dynamics simulations, and experimental results on silica nanopores by Schreiber et al. (2001). MD, molecular dynamics; FCC, face-centered cubic. [Color online.]



transition behavior of pore water in the following two aspects: (i) the surface topography may influence the integrity of ice crystals and thus alter the unfrozen water content; (ii) the elastic modulus may have considerable effects on the confinements because the water freezing expansion needs to overcome the hoop stress provided by the solid. With the most common FCC crystal structure, this study highlighted that the Young–Laplace equation does not hold in the low temperature range, identified the existence of the “unfreezable temperature threshold”, and provided a pathway to quantify the temperature depression effects in nanopores.

The predicted melting points are directly associated with matric suction via eq. (1). In this sense, this work can be regarded as an indirect way to determine matric suction in nanopores. From a thermodynamics viewpoint, matric suction (or negative matric potential) can be defined as the free energy change in a unit volume of water when being transferred reversibly and isothermally from a soil water state (i.e., pore water in soil matrix) to a free water state (i.e., pure bulk water state) (Slatyer and Taylor 1960; Noy-Meir and Ginzburg 1967). Therefore, the calculation of free energy landscapes, which is computationally expensive, is inevitable for direct determination of matric suction via molecular simulations. Based on metadynamics (Laio and Parrinello 2002), a powerful algorithm to enhance the sampling process in MD, a framework to determine matric potential via molecular simulations was developed in Zhang et al. (2017a). Although metadynamics can speed up the sampling process, a simulation case involving several water molecules takes more than 1 month, indicating the computational costs are still very expensive. Consequently, in practice, this framework is only applicable to a limited number of water molecules, i.e., in the tightly adsorbed regime of SWCCs. Due to the consideration, this technique is not adopted in the current study. However, from a different angle, this study can provide an indirect estimation of matric suction up to the transition regime of capillarity and adsorption in SWCCs.

Summary and conclusions

The physical mechanisms underlying the PCC of frozen soils in the low temperature range are complicated due to the complex interplay of adsorption and capillarity. It is hypothesized that the phase behavior of water confined in nano-size pores controls the PCC in the low temperature range. To unravel the potential phys-

ical mechanisms, molecular dynamics simulation was employed to investigate the phase behavior of water confined in nanopores in this study. An mW model was adopted to depict the interatomic potentials of water while a perforated mineral with an FCC crystal structure was selected to represent the soil matrix. The wettability of the nanopore was controlled by adjusting the water–nanopore interaction energy. A specific simulation procedure was developed for determining the melting point.

Major simulation results are summarized in the following. The increase of wettability of nanopore leads to an increase the unfrozen water content at T_c and may slightly increase the melting point by 4 K. The melting point increases with the increase of nanopore diameter while the unfrozen water content at T_c decreases. The water confined in the nanopores with a diameter of 1 and 2 nm cannot form ice crystals, which is attributable to the dominant adsorptive effect. Compared with the simulation and documented experimental results, the Young–Laplace–Clapeyron method underestimates the temperature depression by 22–25 K and overlooks the “unfreezable temperature threshold”.

This study provided a pathway to quantify the temperature depression effects in nanopores via molecular dynamics. It is highlighted that adsorption is not negligible in the low temperature range and there exists an “unfreezable temperature threshold” that is missing in the conventional ways to formulate PCC. Based on these findings, it is concluded that the Young–Laplace equation may not well apply in the low temperature range.

Acknowledgements

The financial support from the National Science Foundation (NSF CMMI 1562522) and the Michigan Space Grant Consortium is gratefully acknowledged. We also acknowledge Superior, a high-performance computing cluster at Michigan Technological University, for providing computational resources to fulfill this study. The insightful and constructive comments provided by the Editor and two anonymous reviewers are appreciated by the authors.

References

- Alba-Simionesco, C., Coasne, B., Dosseh, G., Dudziak, G., Gubbins, K.E., Radhakrishnan, R., and Sliwinska-Bartkowiak, M. 2006. Effects of confinement on freezing and melting. *Journal of Physics: Condensed Matter*, **18**(6): R15. doi:10.1088/0953-8984/18/6/R01.
- Amarasinghe, P.M., and Anandarajah, A. 2011. Influence of fabric variables on clay–water–air capillary meniscus. *Canadian Geotechnical Journal*, **48**(7): 987–995. doi:10.1139/t11-018.
- Anandarajah, A., and Amarasinghe, P.M. 2011. Microstructural investigation of soil suction and hysteresis of fine-grained soils. *Journal of Geotechnical and Geoenvironmental Engineering*, **138**(1): 38–46. doi:10.1061/(ASCE)GT.1943-5606.0000555.
- Anderson, D.M. 1967. The interface between ice and silicate surfaces. *Journal of Colloid and Interface Science*, **25**(2): 174–191. doi:10.1016/0021-9797(67)90021-5.
- Anderson, D.M., and Hoekstra, P. 1965. Crystallization of clay-adsorbed water. *Science*, **149**(3681): 318–319. doi:10.1126/science.149.3681.318. PMID:17838109.
- Bachmann, J.J., and van der Ploeg, R.R. 2002. A review on recent developments in soil water retention theory: interfacial tension and temperature effects. *Journal of Plant Nutrition and Soil Science*, **165**(4): 468. doi:10.1002/1522-2624(200208)165:4<468::AID-JPLN468>3.0.CO;2-G.
- Berendsen, H.J.C., Postma, J.P.M., van Gunsteren, W.F., and Hermans, J. 1981. Interaction models for water in relation to protein hydration. *In* *Intermolecular forces*. pp. 331–342. Springer. doi:10.1007/978-94-015-7658-1_21.
- Berendsen, H.J.C., Grigera, J.R., and Straatsma, T.P. 1987. The missing term in effective pair potentials. *The Journal of Physical Chemistry*, **91**(24): 6269–6271. doi:10.1021/j100308a038.
- Bourg, I.C., and Sposito, G. 2010. Connecting the molecular scale to the continuum scale for diffusion processes in smectite-rich porous media. *Environmental Science & Technology*, **44**(6): 2085–2091. doi:10.1021/es903645a. PMID:20146523.
- Çengel, Y.A., and Boles, M.A. 2004. *Thermodynamics: an engineering approach*. 5th ed. McGraw-Hill, New York.
- Cheng, S., and Robbins, M.O. 2014. Capillary adhesion at the nanometer scale. *Physical Review E*, **89**(6): 62402. doi:10.1103/PhysRevE.89.062402.
- De La Llave, E., Molinero, V., and Scherlis, D.A. 2012. Role of confinement and surface affinity on filling mechanisms and sorption hysteresis of water in nanopores. *The Journal of Physical Chemistry C*, **116**(2): 1833–1840. doi:10.1021/jp206580z.
- Faken, D., and Jónsson, H. 1994. Systematic analysis of local atomic structure

- combined with 3D computer graphics. *Computational Materials Science*, **2**(2): 279–286. doi:10.1016/0927-0256(94)90109-0.
- Findenegg, G.H., Jähnert, S., Akcakayiran, D., and Schreiber, A. 2008. Freezing and melting of water confined in silica nanopores. *ChemPhysChem*, **9**(18): 2651–2659. doi:10.1002/cphc.200800616. PMID:19035394.
- Gonzalez Solveyra, E., De La Llave, E., Scherlis, D.A., and Molinero, V. 2011. Melting and crystallization of ice in partially filled nanopores. *The Journal of Physical Chemistry B*, **115**(48): 14196–14204. doi:10.1021/jp205008w. PMID:21863824.
- Honeycutt, J.D., and Andersen, H.C. 1987. Molecular dynamics study of melting and freezing of small Lennard-Jones clusters. *The Journal of Physical Chemistry*, **91**(19): 4950–4963. doi:10.1021/j100303a014.
- Ichikawa, Y., Kawamura, K., Fujii, N., and Nattavut, T. 2002. Molecular dynamics and multiscale homogenization analysis of seepage/diffusion problem in bentonite clay. *International Journal for Numerical Methods in Engineering*, **54**(12): 1717–1749. doi:10.1002/nme.488.
- Iwata, S., Tabuchi, T., and Warkentin, B.P. 1995. Soil-water interactions: Mechanisms and applications. 2nd ed. Marcel Dekker, Inc.
- Jorgensen, W.L., Chandrasekhar, J., Madura, J.D., Impey, R.W., and Klein, M.L. 1983. Comparison of simple potential functions for simulating liquid water. *The Journal of Chemical Physics*, **79**(2): 926–935. doi:10.1063/1.445869.
- Katti, D.R., Schmidt, S.R., Ghosh, P., and Katti, K.S. 2007. Molecular modeling of the mechanical behavior and interactions in dry and slightly hydrated sodium montmorillonite interlayer. *Canadian Geotechnical Journal*, **44**(4): 425–435. doi:10.1139/t06-127.
- Katti, D.R., Srinivasamurthy, L., and Katti, K.S. 2015. Molecular modeling of initiation of interlayer swelling in Na-Montmorillonite expansive clay. *Canadian Geotechnical Journal*, **52**(9): 1385–1395. doi:10.1139/cgj-2014-0309.
- Koga, K., Gao, G.T., Tanaka, H., and Zeng, X.C. 2001. Formation of ordered ice nanotubes inside carbon nanotubes. *Nature*, **412**(6849): 802–805. doi:10.1038/35090532. PMID:11518961.
- Konrad, J.-M., and Morgenstern, N.R. 1980. A mechanistic theory of ice lens formation in fine-grained soils. *Canadian Geotechnical Journal*, **17**(4): 473–486. doi:10.1139/t80-056.
- Konrad, J.-M., and Morgenstern, N.R. 1981. The segregation potential of a freezing soil. *Canadian Geotechnical Journal*, **18**(4): 482–491. doi:10.1139/t81-059.
- Koopmans, R.W.R., and Miller, R.D. 1966. Soil freezing and soil water characteristic curves. *Soil Science Society of America Journal*, **30**(6): 680–685. doi:10.2136/sssaj1966.03615995003000060011x.
- Laio, A., and Parrinello, M. 2002. Escaping free-energy minima. *Proceedings of the National Academy of Sciences*, **99**(20): 12562–12566. doi:10.1073/pnas.202427399.
- Laplace, P.S. 1806. Supplement to book 10 of *Mécanique Céleste*. Crapelet, Courcier, Bachelier, Paris.
- Likos, W.J., and Yao, J. 2014. Effects of constraints on van Genuchten parameters for modeling soil-water characteristic curves. *Journal of Geotechnical and Geoenvironmental Engineering*, **140**(12): 06014013. doi:10.1061/(ASCE)GT.1943-5606.0001168.
- Liu, W.K., Karpov, E.G., Zhang, S., and Park, H.S. 2004. An introduction to computational nanomechanics and materials. *Computer Methods in Applied Mechanics and Engineering*, **193**(17–20): 1529–1578. doi:10.1016/j.cma.2003.12.008.
- Liu, Z., and Yu, X. 2013. Physically based equation for phase composition curve of frozen soils. *Transportation Research Record: Journal of the Transportation Research Board*, **2349**: 93–99. doi:10.3141/2349-11.
- Liu, Z., Muldrew, K., Wan, R.G., and Elliott, J.A.W. 2003. Measurement of freezing point depression of water in glass capillaries and the associated ice front shape. *Physical Review E*, **67**(6): 061602. doi:10.1103/PhysRevE.67.061602.
- Lu, N., and Likos, W.J. 2004. *Unsaturated soil mechanics*. John Wiley & Sons.
- Luan, B., and Robbins, M.O. 2005. The breakdown of continuum models for mechanical contacts. *Nature*, **435**(7044): 929–932. doi:10.1038/nature03700. PMID:15959512.
- Martínez, L., Andrade, R., Birgin, E.G., and Martínez, J.M. 2009. PACKMOL: a package for building initial configurations for molecular dynamics simulations. *Journal of Computational Chemistry*, **30**(13): 2157–2164. doi:10.1002/jcc.21224. PMID:19229944.
- McQueen, I.S., and Miller, R.F. 1974. Approximating soil moisture characteristics from limited data: empirical evidence and tentative model. *Water Resources Research*, **10**(3): 521–527. doi:10.1029/WR010i003p00521.
- Mitchell, J.K., and Soga, K. 2005. *Fundamentals of soil behavior*. John Wiley & Sons.
- Molinero, V., and Moore, E.B. 2009. Water modeled as an intermediate element between carbon and silicon. *The Journal of Physical Chemistry B*, **113**(13): 4008–4016. doi:10.1021/jp805227c. PMID:18956896.
- Moore, E.B., and Molinero, V. 2011. Structural transformation in supercooled water controls the crystallization rate of ice. *Nature*, **479**(7374): 506–508. doi:10.1038/nature10586. PMID:22113691.
- Moore, E.B., de La Llave, E., Welke, K., Scherlis, D.A., and Molinero, V. 2010. Freezing, melting and structure of ice in a hydrophilic nanopore. *Physical Chemistry Chemical Physics*, **12**(16): 4124–4134. doi:10.1039/b919724a. PMID:20379503.
- Moore, E.B., Allen, J.T., and Molinero, V. 2012. Liquid-ice coexistence below the melting temperature for water confined in hydrophilic and hydrophobic nanopores. *The Journal of Physical Chemistry C*, **116**(13): 7507–7514. doi:10.1021/jp3012409.
- Mualem, Y. 1976. A new model for predicting the hydraulic conductivity of unsaturated porous media. *Water Resources Research*, **12**(3): 513–522. doi:10.1029/WR012i003p00513.
- Noy-Meir, I., and Ginzburg, B.Z. 1967. An analysis of the water potential isotherm in plant tissue I. The theory. *Australian Journal of Biological Sciences*, **20**(4): 695. doi:10.1071/BI9670695.
- Or, D., and Tuller, M. 1999. Liquid retention and interfacial area in variably saturated porous media: upscaling from single-pore to sample-scale model. *Water Resources Research*, **35**(12): 3591–3605. doi:10.1029/1999WR900262.
- Painter, S.L., and Karra, S. 2014. Constitutive model for unfrozen water content in subfreezing unsaturated soils. *Vadose Zone Journal*, **13**(4). doi:10.2136/vzj2013.04.0071.
- Plimpton, S. 1995. Fast parallel algorithms for short-range molecular dynamics. *Journal of Computational Physics*, **117**(1): 1–19. doi:10.1006/jcph.1995.1039.
- Plimpton, S., Crozier, P., and Thompson, A. 2007. LAMMPS-large-scale atomic/molecular massively parallel simulator. Sandia National Laboratories, Vol. 18.
- Schreiber, A., Ketelsen, I., and Findenegg, G.H. 2001. Melting and freezing of water in ordered mesoporous silica materials. *Physical Chemistry Chemical Physics*, **3**(7): 1185–1195. doi:10.1039/b010086m.
- Sheng, D., Zhang, S., Yu, Z., and Zhang, J. 2013. Assessing frost susceptibility of soils using PCHeave. *Cold Regions Science and Technology*, **95**: 27–38. doi:10.1016/j.coldregions.2013.08.003.
- Slatyer, R.O., and Taylor, S.A. 1960. Terminology in plant- and soil-water relations. *Nature*, **187**(4741): 922–924. doi:10.1038/187922a0.
- Song, C.R., Cho, H., Jung, Y.-H., Cheng, A.H.-D., Al-Ostaz, A., and Alostaz, A. 2007. Bridging molecular, particulate and continuum mechanics for geomechanics application. In *Advances in measurement and modeling of soil behavior*. American Society of Civil Engineers, Reston, Va. pp. 1–10. doi:10.1061/40917(236)33.
- Spaans, E.J.A., and Baker, J.M. 1996. The soil freezing characteristic: Its measurement and similarity to the soil moisture characteristic. *Soil Science Society of America Journal*, **60**(1): 13–19. doi:10.2136/sssaj1996.03615995006000010005x.
- Stillinger, F.H., and Weber, T.A. 1985. Computer simulation of local order in condensed phases of silicon. *Physical Review B*, **31**(8): 5262–5271. doi:10.1103/PhysRevB.31.5262.
- Stukowski, A. 2010. Visualization and analysis of atomistic simulation data with OVITO—the Open Visualization Tool. *Modelling and Simulation in Materials Science and Engineering*, **18**(1): 015012. doi:10.1088/0965-0393/18/1/015012.
- Watanabe, K., and Flury, M. 2008. Capillary bundle model of hydraulic conductivity for frozen soil. *Water Resources Research*, **44**(12): 1–9. doi:10.1029/2008WR007012.
- Webb, S.W. 2000. A simple extension of two-phase characteristic curves to include the dry region. *Water Resources Research*, **36**(6): 1425–1430. doi:10.1029/2000WR900057.
- Williams, P.J., and Smith, M.W. 1989. *The frozen earth*. Cambridge University Press.
- Young, T. 1805. An essay on the cohesion of fluids. *Philosophical Transactions of the Royal Society of London*, **95**: 65–87. doi:10.1098/rstl.1805.0005.
- Zhang, C., Liu, Z., and Deng, P. 2016a. Contact angle of soil minerals: a molecular dynamics study. *Computers and Geotechnics*, **75**: 48–56. doi:10.1016/j.compgeo.2016.01.012.
- Zhang, C., Liu, Z., and Deng, P. 2016b. Atomistic-scale investigation of effective stress principle of saturated porous materials by molecular dynamics. *Geophysical Research Letters*, **43**(19): 10,257–10,265. doi:10.1002/2016GL070101.
- Zhang, S., Sheng, D., Zhao, G., Niu, F., and He, Z. 2016c. Analysis of frost heave mechanisms in a high-speed railway embankment. *Canadian Geotechnical Journal*, **53**(3): 520–529. doi:10.1139/cgj-2014-0456.
- Zhang, C., Dong, Y., and Liu, Z. 2017a. Lowest matric potential in quartz: Meta-dynamics evidence. *Geophysical Research Letters*, **44**(4): 1706–1713. doi:10.1002/2016GL071928.
- Zhang, C., Liu, Z., and Dong, Y. 2017b. Effects of adsorptive water on the rupture of nanoscale liquid bridges. *Applied Clay Science*, **146**(July): 487–494. doi:10.1016/j.clay.2017.07.002.
- Zhang, T., Barry, R.G., Knowles, K., Ling, F., and Armstrong, R.L. 2003. Distribution of seasonally and perennially frozen ground in the Northern Hemisphere. In *Proceedings of the 8th International Conference on Permafrost*, Zurich, Switzerland. A.A. Balkema, the Netherlands. Vol. 2, 1289–1294.